INTERNATIONAL JOURNAL FOR NUMERICAL AND ANALYTICAL METHODS IN GEOMECHANICS
Int. J. Numer. Anal. Meth. Geomech., **22**, 983–1000 (1998)

EFFICIENT SOLUTION OF 3-D GEOMECHANICAL PROBLEMS BY INDIRECT BEM USING ITERATIVE METHODS

M. A. KAYUPOV[1,*], V. E. BULGAKOV[2] AND G. KUHN[1]

[1] *Lehrstuhl für Technische Mechanik, Universität Erlangen-Nürnberg, Egerlandstr. 5, D-91058 Erlangen, Germany*
[2] *Department of Applied Mathematics, Moscow State University of Civil Engineering, Yaroslavskoe Shosse 26, Moscow, 129337, Russia*

SUMMARY

The research herein primarily addresses to geomechanical problems of underground constructions in Mining and Civil Engineering. The problems are solved using the Indirect Boundary Element Method (IBEM). Although the geometry of the constructions themselves is usually very complicated, it will become much more complicated if we were to draw the existing joints. The computational problem therefore is how to deal with huge amount of equations and find out efficient methods of their formation and solution keeping in mind restraints of the computer memory and calculation time. Several approaches are used to enhance the performance of the Indirect Boundary Element Method. One of them deals with application of efficient equation solvers. It is shown that Krylov-type methods like CGS and GMRES with simple Jacoby preconditioning appear to be efficient and robust. In addition, adaptive integration on the boundary elements, together with diagonal dominance of equations make it possible to accelerate convergence of the iterative procedure. Some of the problems discussed allow a substantial reduction of matrix entries that leads to a very cheap iterative solution keeping reasonable accuracy of the results. © 1998 John Wiley & Sons, Ltd.

Key words: geomechanics; indirect boundary element method (BEM); three-dimensional (3-D) elastostatics; iterative methods; approximate solution

INTRODUCTION

Historically, operational experience and mining intuition play a decisive role in finding a suitable method of mining. Since many different factors (such as economics, the type of the deposit to be extracted, machinery, the qualification of the personnel, etc.) have to be taken into consideration, the experts' assessments are at present the only way to define the method of mining during the first stages of the mine design. Once the mining method is defined the Geomechanics has to provide optimal parameters required for the underground excavations. For example, if the room-and-pillar mining method is chosen, the Industry is interested in the optimal order for conducting mining operations, e.g. the already extracted areas must not have any negative influence on the area to be extracted. The main desired parameters are shapes and sizes of the

*Correspondence to: Dr. M. A. Kayupov, Lehrstuhl für Technische Mechanik, Universität Erlangen-Nürnberg, Egerlandstr. 5, D-91058 Erlangen, Germany.

CCC 0363–9061/98/120983–18$17.50

Received 26 September 1997
Revised 30 January 1998

pillars. In this particular case, the deposit is to be extracted with minimum losses of minerals used in the pillars. If the pillars are massive then a lot of the minerals will be wasted underground. However, if the pillars are too weak the price for this will be in the loss of people's lives and more minerals will be lost due to accidents. Thus, it is extremely important to have efficient methods for analysis and prediction of the regions around excavations where the rock may be overstressed and threaten the mining operation.

The rock mass with the excavations represents a peculiar mechanical construction. This is why the use of the Optimal Structural Design Methods seem to be a natural step for creating reliable and stable underground excavations. In fact, the development of methods which allow a decrease of breaking stress concentrations in the rock mass is equivalent to the solution of the optimal design problem to create a construction of a maximum strength; the decreasing of minerals losses in pillars is equivalent to the shape optimal design of the structure of the minimum weight and the like. At present, the Optimal Structural Design Methods find wide application in Mechanical Engineering, and the progress made in this direction allows us to concentrate on the efficiency of using these methods in the mine design. However, should we decide to apply the Optimal Design Methods in Geomechanics we must remember that as opposed to artificial constructions which are built of the materials with well-known properties the rock mass itself is an extremely complicated physical object.

The designer is able to choose the suitable materials to create the construction while the Mechanical Engineering objects are considered. At least, the designer can order the production of the materials with necessary properties. As against, the rock mass properties are set by the Nature, and the limited methods that can be employed to find out or improve these properties are usually too expensive to be used in the ordinary mine projects. Therefore, the most suitable application of the Optimal Design Methods in Geomechanics deals with the development of the Shape Optimisation. As the first step, we need here an efficient method to estimate stress field close to excavations that usually have a complicated geometry. Because rock mass stability deals with fracture propagation and rock block movements along joints, it is also very important to be able to model the joints explicitly. Thus, finally, we can expect the model with very complicated geometry and, therefore, we need efficient numerical methods for the problem solution.

Various methods are used in Geomechanics for solving these problems. The Indirect Boundary Element Method (IBEM) is one of them.[1–8] This method is preferred for geometrically complex geotechnical problems with large numbers of interacting excavations and jointed rock mass. It is explained by the fact that only the boundary of the region and joints to be analysed need to be discretized. However, even with the BEM, large number of algebraic equations need to be formed and solved, which imposes restrictions upon the size of problem. Thus, if we wish to model complicated geotechnical situations, special computational schemes must be employed.

One of such schemes includes the use of advanced iterative solvers in the IBEM-based codes. First of all, iterative methods do not change the coefficients in the equations during their solution. Thus, it is not necessary to recalculate the whole matrix on each step of shape optimization or fracture propagation. In case of optimal shape design using the Local Variation Method, we change only several rows and columns at a single step of the optimization procedure.[1] Fracture propagation similarly results in adding rows and columns in the matrix in each step of crack increment. In addition, we can use the solution of the previous step as an initial approach to the next one. On the contrary, if we use direct methods to solve the simultaneous equations we need either conduct the whole matrix recalculation, or store additionally an initial matrix. However, in contrast to the direct methods iterative solvers show their maximum efficiency if special rules are

used to form the matrix. In this study, we demonstrate how adaptive integration on the boundary elements makes it possible to accelerate convergence of the iterative procedure. It is shown that Krylov-type methods like CGS and GMRES with simple Jacoby preconditioning appear to be efficient and robust.

Although the above problems can be approximated using huge amount of boundary elements, a significant part of them have rather weak interaction because of the fact that displacements and, especially stresses decay fast away from the point of application of fictitious load. Some of the problems discussed in the paper allow a substantial reduction of matrix entries that leads to a very cheap iterative solution keeping reasonable accuracy of the results. This motivates further investigation on *a priori* estimates of small matrix entries which can be neglected aimed to savings of the computer memory requirements.

INDIRECT BOUNDARY ELEMENT METHOD

In accordance with the IBEM technique,[1–3] it is assumed that the space inside of the excavations and fractures is filled up with material with the same elastic properties as the rock mass. That is, an infinite homogeneous medium without any cavities is considered. The surfaces are divided into small boundary elements. So, each element, representing a part of the surface as a geometrical object, is situated in the infinite homogeneous medium with elastic properties of the rock mass. This approach allows the use of known fundamental solutions for loads acting in infinite medium. Assuming that uniformly distributed load acts on every boundary element, an initial problem is reduced to finding out such load distribution, which satisfies boundary conditions. Thus, appropriate loading of boundary elements allows one to model excavations and fractures, when stresses and displacements in the rock mass with these entities are the same as in infinite elastic medium without the excavations and fractures, but with loaded boundary elements.

Stresses $\sigma_x, \sigma_y, \ldots, \tau_{yz}$ at an arbitrary point of the medium are defined as superposition of stresses in the virgin rock mass and stresses due to loaded boundary elements. Displacements u_x, u_y, u_z due to excavations and growing fractures are defined analogously, but in this case, displacements in the virgin rock mass are assumed to be equal to zero

$$\begin{aligned}
\sigma_x &= \sigma_x^{\circ} + \sum_{i=1}^{N} (a_{xxxi} q_{xi} + a_{xxyi} q_{yi} + a_{xxzi} q_{zi}) \\
&\vdots \\
\tau_{yz} &= \tau_{yz}^{\circ} + \sum_{i=1}^{N} (a_{yzxi} q_{xi} + a_{yzyi} q_{yi} + a_{yzzi} q_{zi}) \\
&\vdots \\
u_z &= \sum_{i=1}^{N} (b_{zzxi} q_{xi} + b_{zzyi} q_{yi} + a_{zzzi} q_{zi})
\end{aligned} \tag{1}$$

where N is total amount of boundary elements; q_{xi}, q_{yi}, q_{zi} are projections of the fictitious load $\mathbf{q}_i$ acting on the element with number i on axes Ox, Oy and Oz of the global Cartesian system of co-ordinates $Oxyz$, respectively; a_{xxxi} is the value of stress σ_x at point W due to unit load q_{xi} on the element with number i, a_{xxyi} is the value of stress σ_x at point W due to unit load q_{yi} on the element with number i, etc.

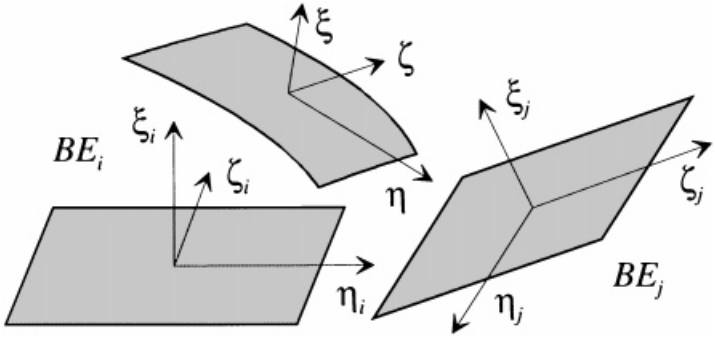

Figure 1. Local systems of co-ordinates on boundary elements (BE)

If we consider traction boundary conditions then stresses on the surfaces are defined as follows:

$$\begin{aligned}
\sum_{i=1}^{N} (a_{\xi\xi xi} q_{xi} + a_{\xi\xi yi} q_{yi} + a_{\xi\xi zi} q_{zi}) &= \sigma_{\xi}^{\mathrm{b}} - \sigma_{\xi}^{\mathrm{o}} \\
\sum_{i=1}^{N} (a_{\xi\eta xi} q_{xi} + a_{\xi\eta yi} q_{yi} + a_{\xi\eta zi} q_{zi}) &= \tau_{\xi\eta}^{\mathrm{b}} - \tau_{\xi\eta}^{\mathrm{o}} \\
\sum_{i=1}^{N} (a_{\xi\zeta xi} q_{xi} + a_{\xi\zeta yi} q_{yi} + a_{\xi\zeta zi} q_{zi}) &= \tau_{\xi\zeta}^{\mathrm{b}} - \tau_{\xi\zeta}^{\mathrm{o}}
\end{aligned} \tag{2}$$

or, in matrix notation,

$$\mathbf{Aq} = \mathbf{b},$$

where $\sigma_{\xi}^{\mathrm{o}}$, $\tau_{\xi\eta}^{\mathrm{o}}$, $\tau_{\xi\zeta}^{\mathrm{o}}$ are stresses in the virgin rock mass for local Cartesian system of co-ordinates $\xi\,\eta\,\zeta$ with axis ξ perpendicular to the surface of the excavation (Figure 1); values $\sigma_{\xi}^{\mathrm{b}}$, $\tau_{\xi\eta}^{\mathrm{b}}$, $\tau_{\xi\zeta}^{\mathrm{b}}$ represent traction boundary conditions and construct together with stresses $\sigma_{\xi}^{\mathrm{o}}$, $\tau_{\xi\eta}^{\mathrm{o}}$, $\tau_{\xi\zeta}^{\mathrm{o}}$ vector **b**; $a_{\xi\xi xi}$ is the value of stress σ_{ξ} on the excavation or fracture surface due to unit fictitious load q_{xi} on the element with number i, $a_{\xi\xi yi}$ is the value of stress σ_{ξ} on the surface due to unit fictitious load q_{yi} on the element with number i, etc. Coefficients $a_{\xi\xi xi}$, $a_{\xi\xi yi}$, … , $a_{\xi\zeta zi}$ compose matrix **A** of the system (2). Simultaneous equations (2) are used to define unknown fictitious loads q_{xi}, q_{yi}, q_{zi} $(i = 1, 2, \ldots, N)$ that form vector of unknowns **q**. Once equations (2) are solved, stresses and displacements on the excavation and fracture surfaces or at inner points of the rock mass are calculated by using formulae (1).

ITERATIVE SOLUTION OF IBEM EQUATIONS

One of the drawbacks of BEM (IBEM) systems compared to usual Finite Element Method (FEM) systems is that they are not sparse. Therefore, when performing iterations the full matrix is involved into computations in each iterative step which imposes a strong limit upon the number of iterations in order to keep solution procedure efficient. This limit is much stronger than that of FE analysis where performing 1–5 thousand iterations might be still efficient compared to a direct method application. Another drawback of BEM systems is their non-symmetry and non-positive

definiteness. These features complicate obtaining rigorous theoretical estimates for prediction of iterative methods convergence except that for some particular cases. On the other hand, system matrix properties are strongly influenced by the use of Kelvin's fundamental solution for computing matrix entries which can be seen from the following expressions[9] for tractions $\mathbf{t}_n$ and displacements $\mathbf{u}$ at the point x_1, y_1, z_1 due to force $\mathbf{Q}$ applied at point x_2, y_2, z_2

$$\mathbf{t}_n = -\frac{1-2\nu}{8\pi(1-\nu)R^2}\left[-(\mathbf{r}\cdot\mathbf{Q})\mathbf{n} + (\mathbf{n}\cdot\mathbf{Q})\mathbf{r} + \mathbf{Q}(\mathbf{n}\cdot\mathbf{r}) + \frac{3}{1-2\nu}(\mathbf{r}\cdot\mathbf{Q})(\mathbf{n}\cdot\mathbf{r})\mathbf{r}\right]$$

$$\mathbf{u} = -\frac{1+\nu}{8\pi E(1-\nu)R}\left[-(3-4\nu)\mathbf{Q} + \mathbf{r}(\mathbf{r}\cdot\mathbf{Q})\right]$$

where $\mathbf{r} = \mathbf{R}/R$,

$$\mathbf{R} \equiv \mathbf{R}\{x_1 - x_2, y_1 - y_2, z_1 - z_2\}$$

$$R = \sqrt{(x_1 - x_2)^2 + (y_1 - y_2)^2 + (z_1 - z_2)^2}$$

Here, E and ν are Young's modulus and Poisson's ratio, respectively, $\mathbf{n}$ is a unit normal to some surface element. Because values of $\mathbf{t}_n$ and $\mathbf{u}$ decrease rather quickly (as $O(R^{-2})$ and $O(R^{-1})$ for stresses and displacements, respectively), when the distance R is increased then these properties suggest certain possibilities to solve the systems of equations efficiently.

It was recently discovered that in many BEM applications Lanczos-type (or Krylov subspace) iterative methods such as CGS, and GMRES methods described in pioneering works[10–12] with simple diagonal or block-diagonal preconditioning converge well. These methods were originally created as an efficient tool for solving iteratively sparse systems arising in finite-difference and FE applications. In References 13–15 and other works, Krylov methods were tested for BEM elasticity and heat conduction problems, in Reference 16 for Navier–Stokes equations. In Reference 17, Krylov methods have been applied to large practical BEM elasticity and heat conduction problems. Extensive numerical experiments demonstrated that the direct application of iterative methods to BEM collocation systems has the following drawbacks. In some cases for elasticity problems with unstructured meshes and small aspect ratio, convergence of preconditioned GMRES and CGS methods was very slow. Solution efficiency of problems which size does not fit computer main memory was substantially reduced. Although processor capacities of new workstations are satisfactory for large BEM problems the growth of computers random access memory is rather slow. Besides, due to the n^2 asymptotic of storing dense matrix coefficients, memory requirements increase to the power of 2 with increase of the problem size. The disk-memory exchange is very slow compared to the speed of arithmetic operations and need principal changes in data storage devices. The use of modern supercomputers is very expensive and still inefficient for large BEM problems.

We can refer to References 10 and 11 and to many other issues for the description of CGS and GMRES methods. In our case the resolution matrices of IBEM are scaled row-wise with respect to main diagonal entries which corresponds to the Jacoby preconditioning and we use no preconditioning in iterations for these matrices. Strong convergence estimates are not worked out for these methods. Nevertheless, it is known that the smaller number of matrix eigenvalues are on the left-half of the complex plane the better convergence of Krylov methods can be expected (see e.g. References 10 and 18). This was demonstrated in References 17 and 19 experimentally for not diagonally dominant matrices. In this study it is shown that using an adaptive integration

technique for IBEM with constant elements especially for problems with traction boundary conditions which are typical in mining engineering applications, a diagonal predominance of the matrix can be substantially improved. This is very important for convergence of practically all known iterative methods. From the well known Gershgorin theorem one can obtain that

$$\exists i \, |\lambda(\mathbf{A}) - 1| \leqslant \rho_i$$

where $\lambda(\mathbf{A})$ are matrix eigenvalues and $\rho_i = \sum_{j=1;\, j \neq i}^{3N} |a_{ij}/a_{ii}|$. It trivially follows from here that in strongly diagonally dominant scaled matrices all eigenvalues are well clustered around 1 which leads to fast convergent iterative procedures.

ADAPTIVE INTEGRATION TECHNIQUE

To calculate stresses and displacements using formulae (1) or to form matrix for simultaneous equations (2), we need to evaluate joint action of fictitious forces over boundary elements. *The singular behaviour of the fundamental solutions for such forces is a source of known numerical difficulties and errors close to boundaries.* There are several approaches to overcome this problem. One such procedure deals with the use of analytical influence functions that represent the overall performance of each boundary element.[1,2,7,8,20,21] These functions, being derived in closed form, produced distinct advantages over most other approaches employing numerical integration: (1) the analytical influence functions are exact whereas, unknown errors occur during numerical integration, (2) storage requirement is lowered, and computation speed is raised and (3) analytical influence functions can be examined exactly. However, these functions have already got a rather complicated structure for constant flat boundary elements and we may not be optimistic that such functions will soon appear for 3-D non-constant or curve elements even for isotropic elastic media. We may not expect that such complicated work will be carried out for 3-D elements in elastic media with a general anisotropy either. This is because of 3-D closed form solution the Kelvin's problem for such media has not yet been found.

Another approaches deal with different types of self-adapting algorithms of numerical treatment of BEM integrals (see e.g. References 5 and 22 to list a few). In the code MAP3D^{PV}, an automated discretization process optimizes the use of both elements and field points by concentrating them only where results are requested.[23] All of these methods use the fact that stress and displacement functions decreased rather quickly (as $O(R^{-2})$ and $O(R^{-1})$ for stresses and displacements,[9] respectively), when the distance R between the source and observation points is increased. *Although these techniques were primarily created to enhance the BEM performance at points close to boundaries, their implementation at the stage of matrix creation improves matrix properties and, afterwards, convergence of iterative solutions.* We provide some results of relevant numerical modelling in the next section.

In all numerical examples presented in the paper, each boundary element is divided into several subelements by using a technique presented in Reference 5. The amount of subelements on the boundary element depends on the distance between the boundary element and point under consideration. That is, for example, if the point under consideration is situated far from the boundary element and the element is small then the distributed load is substituted by a single fictitious force (Figure 2). If the distance is shorter comparing with the element size then the element is divided into subelements.

To control the process of subdividing and to calculate the amount of subelements we use following technique. In case of the rectangular boundary element, we define amount of

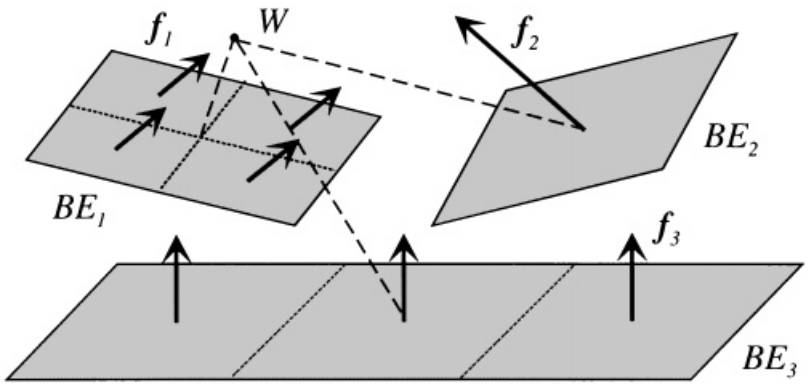

Figure 2. Variation of distribution of fictitious forces at the boundary elements depending on the distances from boundary elements to point W under consideration

subelements n_l along the long side of the boundary element ($n_l \geqslant 1$ is an integer number) using two parameters C_{inf} and $n_{\max}$:

$$n_l = \begin{cases} 1, & \text{if } C_{\text{inf}}(L_{\max}/R) < 1 \\ & C_{\text{inf}}(L_{\max}/R) \\ n_{\max} & \text{if } C_{\text{inf}}(L_{\max}/R) > n_{\max} \end{cases}$$

Parameter $n_{\max}$ is used to define the maximum possible number of subelements along the long side of the boundary element. Parameter C_{inf} is used for correcting the subdividing process (if $C_{\text{inf}} \to \infty$ then all boundary elements were divided into the smallest subelements). Here R is the distance between the point under consideration and the boundary element; $L_{\max}$ is the length of the long side of the boundary element. The amount of subelements along the short side of the boundary element is an integer number $n_s \geqslant 1$ which is defined as $(L_{\min}/L_{\max})\, n_l$, where $L_{\min}$ is the length of the short side of the boundary element. Similar technique is used to subdivide triangular boundary elements. According to Reference 5; in order to provide an appropriate accuracy of results with minimum amount of calculations we set $C_{\text{inf}} = 5$ and define value $n_{\max}$ by the formula

$$n_{\max} = 2\, L_{\max}/R_{\min}$$

where $R_{\min}$ is the minimum distance from the point under consideration and the boundary.

This flexible scheme of calculations allows us to receive accurate numerical results and diminish the calculation time, because only part of the total amount of boundary elements is divided into subelements.

MATRICES WITH PREDOMINANT DIAGONAL ENTRIES

Described above adaptive integration scheme, together with fast decay of kernel functions away from points where fictitious forces are applied, allows us to expect that values of entries in the matrix of the linear equations (2) also decrease while the distance between elements increases. If we take into consideration the local independence of normal and shear stresses due to normal and

shear distributed loads over the boundary for linear elastic isotropic media[24] we may expect predominant diagonal entries in the matrix of the system of equations (2),

$$\sigma_{\xi}^{(\xi)} = \pm 0{\cdot}5q_{\xi}, \quad \sigma_{\eta}^{(\xi)} = \sigma_{\zeta}^{(\xi)} = \pm \frac{v}{2(1-v)} q_{\xi}, \quad \tau_{\xi\eta}^{(\eta)} = \pm 0{\cdot}5q_{\eta}, \quad \sigma_{\xi\zeta}^{(\zeta)} = \pm 0{\cdot}5q_{\zeta} \tag{3}$$

In equations (3), superscript denotes the direction of the fictitious loads and sign ' + ' corresponds to $\xi \to -0$. For flat rectangular boundary element with axes η and ζ parallel to rectangle's sides at the centre of the element all other stress components due to uniformly distributed loads q_{ξ}, q_{η} and q_{ζ} are equal to zero. Thus, to reach the diagonal predominance, we need to use fictitious loads $q_{\xi i}$, $q_{\eta i}$ and $q_{\zeta i}$ corresponding to local co-ordinates $\xi\eta\zeta$ of source elements i (refer Figure 1) rather than loads q_{xi}, q_{yi} and q_{zi}. That is, instead of simultaneous equations (2), we need to form and solve the following ones:

$$\begin{aligned}
&\sum_{i=1}^{N} (a_{\xi\xi\xi i} q_{\xi i} + a_{\xi\xi\eta i} q_{\eta i} + a_{\xi\xi\zeta i} q_{\zeta i}) = \sigma_{\xi}^{b} - \sigma_{\xi}^{o} \\
&\sum_{i=1}^{N} (a_{\xi\eta\xi i} q_{\xi i} + a_{\xi\eta\eta i} q_{\eta i} + a_{\xi\eta\zeta i} q_{\zeta i}) = \tau_{\xi\eta}^{b} - \tau_{\xi\eta}^{o} \\
&\sum_{i=1}^{N} (a_{\xi\zeta\xi i} q_{\xi i} + a_{\xi\zeta\eta i} q_{\eta i} + a_{\xi\zeta\zeta i} q_{\zeta i}) = \tau_{\xi\zeta}^{b} - \tau_{\xi\zeta}^{o}
\end{aligned} \tag{4}$$

where σ_{ξ}^{o}, $\tau_{\xi\eta}^{o}$, $\tau_{\xi\zeta}^{o}$ are stresses in the virgin rock mass for the local Cartesian system of co-ordinates $\xi\eta\zeta$; values σ_{ξ}^{b}, $\tau_{\xi\eta}^{b}$, $\tau_{\xi\zeta}^{b}$ represent traction boundary conditions; $a_{\xi\xi\xi i}$ is the value of stress σ_{ξ} on the excavation or fracture surface due to unit fictitious load $q_{\xi i}$ on the element with number i, $a_{\xi\xi\eta i}$ is the value of stress σ_{ξ} on the surface due to unit fictitious load $q_{\eta i}$ on the element with number i, etc.

The following numerical example allows us to estimate an efficiency of the described methods. Consider $N = 24$ congruent flat rectangular boundary elements that approximate cylinder surface (Figure 3). The diameter of the cylinder is equal to 1 dimensionless unit and the length of the cylinder is equal to 20 units. We assume that the surface represents the boundary of a cavity which is loaded by constant normal dimensionless pressure $P = -1$. Stresses $\sigma_{x}^{o} = \sigma_{y}^{o} = \cdots = \tau_{yz}^{o} = 0$. If the cylinder has the infinite length the problem is a two-dimensional and the circumferential stress σ_{θ} is equal to 1 dimensionless unit. Because the length of the cylinder considered is much larger than its diameter, we may expect quasi-plane strain conditions in the central cross-section of the cylinder.[4]

Figures 4(a) and (b) show surface plots depicted using MAPLE processor[25] of the matrices of 72 simultaneous equations for single fictitious force approximation and adaptively integrated uniformly distributed load, respectively. An existence of a single integration point on each element in the first case results in non-diagonal matrix entries that more than 2 times as much larger than diagonal ones. This prevents convergence of Gauss–Seidel method. However, it takes just 7 iterations to the 10^{6} reduction in the residual vector norm $\|\mathbf{r}\|$, namely

$$\frac{\|\mathbf{r}^{k}\|}{\|\mathbf{b}\|} = \frac{\|\mathbf{A}\mathbf{q}^{k} - \mathbf{b}\|}{\|\mathbf{b}\|} \leqslant \varepsilon = 10^{-6}$$

using GMRES method (Table I). The same tolerance is used in further numerical examples demonstrated in the paper.

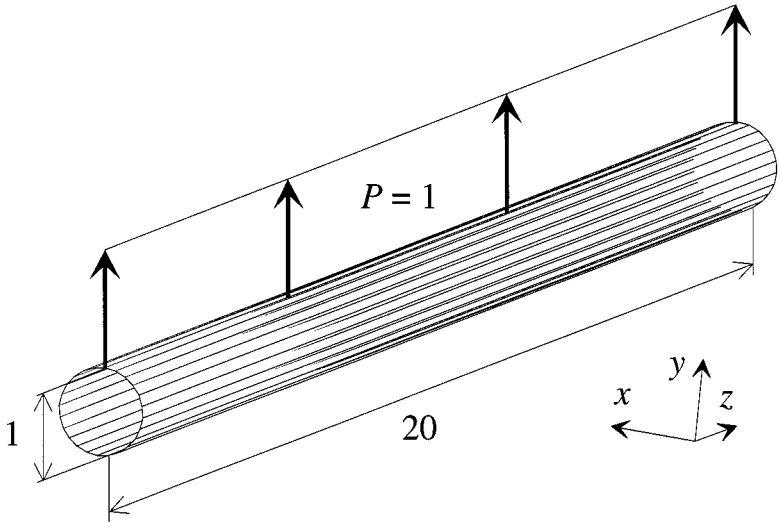

Figure 3. Mesh for quasi-plane strain problem

Adaptive integration of fictitious forces over the elements substantially improves the diagonal predominance of the matrix **A** (Figure 4(b)) and convergence of Gauss–Seidel Method (15 iterations, Table I). It takes only one iteration to get the solution by GMRES method. Circumferential stresses σ_θ are equal to 1·00 in the nodal points at the centres of the boundary elements. Although Gauss elimination scheme takes approximately the same time to calculate the solution as iterative Gauss–Seidel Method for this relatively small problem, an iterative solution of 720 simultaneous equations required 6·2 s of CPU time while the direct method required 436·0 s. However, this numerical example vividly shows an advantage of GMRES method over both direct Gauss elimination scheme and iterative Gauss–Seidel method.

APPROXIMATE SOLUTION

We consider $N = 60$ congruent flat rectangular boundary elements that approximate another cylinder surface (Figure 5). The surface is divided into five sections. The length of each section, that contains 12 boundary elements, is equal to 20 dimensionless units. The diameter of the cylinder is equal to 1 unit. We assume that the surface represents the boundary of a cavity which is loaded by normal dimensionless pressure $P = 0{\cdot}05z$. Stresses $\sigma_x^o = \sigma_y^o = \cdots = \tau_{yz}^o = 0$. The approximation results in 180 simultaneous equations for single fictitious force approximation (Case 1, Figure 6(a)) and adaptively integrated uniformly distributed load (Case 2, Figure 6(b)), respectively. In the first case, as in previous example, Gauss–Seidel method does not converge. It takes 17 and 3 iterations to the 10^6 reduction in the residual vector using GMRES method in Cases 1 and 2, respectively (Table II). Gauss–Seidel Method converges in 14 iterations in Case 2 which takes 0·8s of CPU time. Direct Gauss Elimination Scheme requires 2·5s.

In Figures 6(a) and (b), we can observe that both matrices contain a big amount of small entries. Therefore, it seems to be relevant to discard some of them and try to obtain an appropriate solution with reasonable precision. Investigations devoted to systems with rapidly decreasing

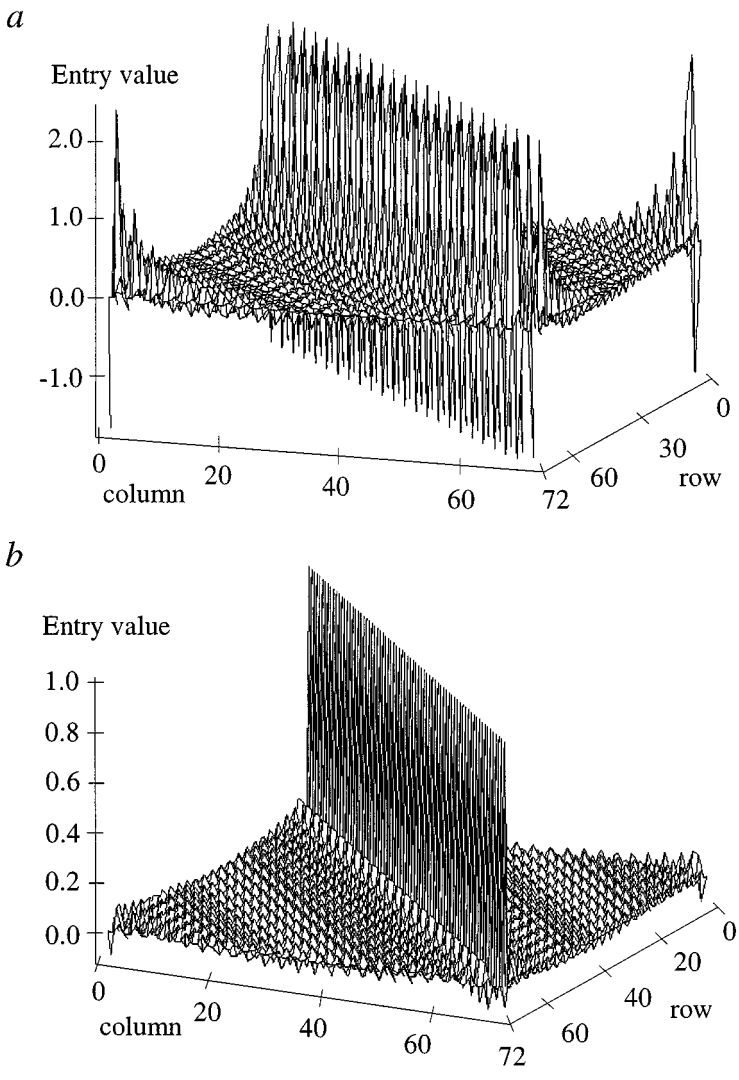

Figure 4. Surface plot of the matrix A containing 72×72 entries. Single fictitious force approximation (a) and adaptive integration (b)

entries can be found in References 26 and 27. In our case, a large amount of small entries is explained by specific features of problems we deal with. Namely, we model extended cavities and, therefore, interaction between elements that approximate different parts of the boundary might be rather small. Let $\bar{\mathbf{q}}$ be an appropriate solution of system (2) obtained from the system.

$$(\mathbf{A} - \mathbf{R})\bar{\mathbf{q}} = \mathbf{b}$$

where $\mathbf{R}$ is the residual matrix containing entries at $\mathbf{A}$ which have been discarded.

Table I. Residuals at different stages of iterative solutions of 72 linear simultaneous equations*

GMRES			Gauss-Seidel method	
Iteration number	Single fictitious force approximation	Adaptive integration	Iteration number	Adaptive integration
1	$2{\cdot}26\times10^{-6}$	$2{\cdot}05\times10^{-7}$	1	0·451
2	$2{\cdot}23\times10^{-6}$		2	$5{\cdot}54\times10^{-2}$
3	$1{\cdot}75\times10^{-6}$		3	$1{\cdot}08\times10^{-2}$
4	$1{\cdot}28\times10^{-6}$		4	$4{\cdot}65\times10^{-3}$
5	$1{\cdot}26\times10^{-6}$		12	$8{\cdot}72\times10^{-6}$
6	$1{\cdot}19\times10^{-6}$		14	$1{\cdot}76\times10^{-6}$
7	$9{\cdot}81\times10^{-7}$		15	$8{\cdot}06\times10^{-7}$

*Computing system by Gauss-Seidel Method and Gauss Elimination Scheme took 0·154 and 0·148 seconds of CPU time, respectively.

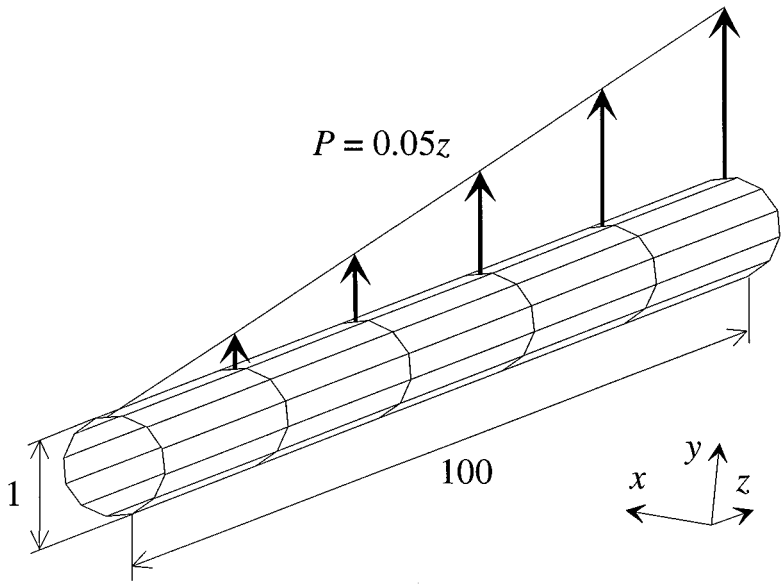

Figure 5. Mesh: long cylinder cavity with internal pressure P

It is easy to get the following estimate for the relative error of the appropriate solution:

$$\frac{\|\mathbf{q}-\bar{\mathbf{q}}\|}{\|\bar{\mathbf{q}}\|} \leqslant \|\mathbf{A}^{-1}\| \cdot \|\mathbf{R}\|$$

Let us use, e.g. the norm

$$\|\mathbf{R}\| = \|\mathbf{R}\|_{\infty} = \max_{i} \sum_{j=1}^{n} |R_{ij}|$$

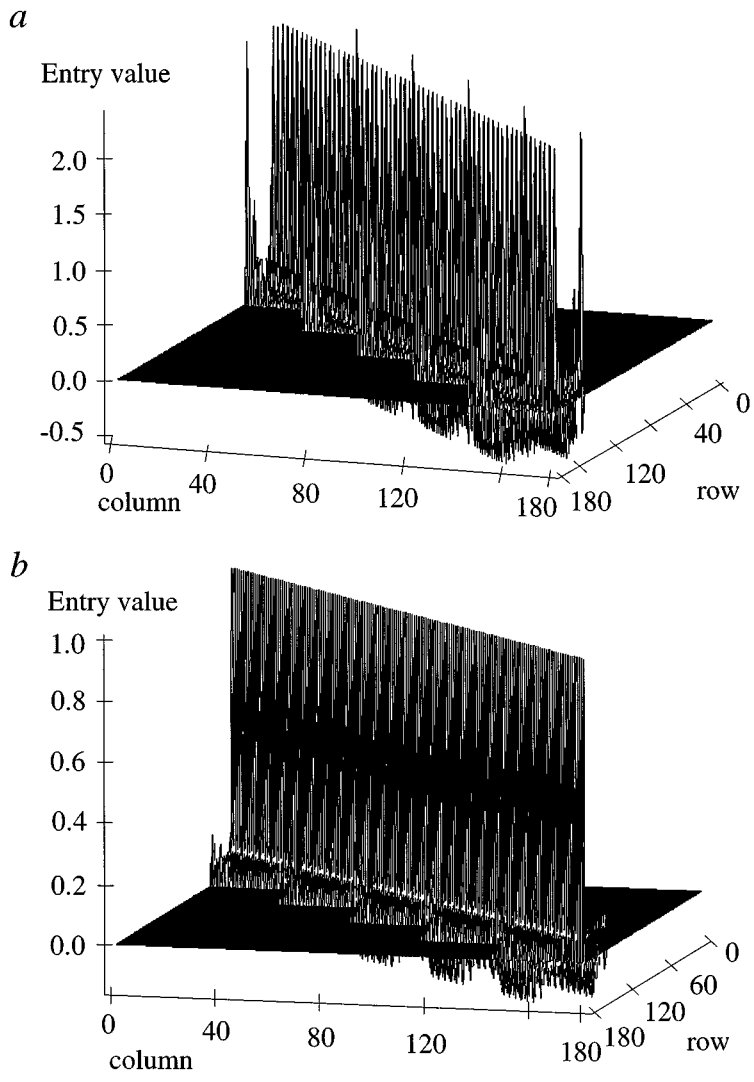

Figure 6. Surface plot of the matrix A containing 180×180 entries. Single fictitious force approximation (a) and adaptive integration (b)

It follows from here that the smaller the entries of **R** the lower error of the approximate solution can be expected. Acceding to the Kelvin's fundamental solution we can estimate $|R_{ij}|$ via $O(R^{-2})$ or $O(R^{-1})$. Therefore, if we have a large amount of entries corresponding to large distances R we expect sufficiently accurate results with substantial savings in matrix–vector multiplications constituting the main operation in iterative methods under consideration.

The most typical problem in mining applications is the problem with known tractions which matrix entries are characterised by the $O(R^{-2})$ asymptotic in 3-D problems. As we usually solve exterior problems with very stretched cavities we can expect a small number of observation points

Table II. Residuals at different stages of iterative solutions of 180 linear simultaneous equations*

	GMRES		Gauss-Seidel method
Iteration number	Single fictitious force approximation	Adaptive integration	
1	$4{\cdot}13\times10^{-5}$	$1{\cdot}21\times10^{-4}$	0·486
2	$9{\cdot}08\times10^{-6}$	$3{\cdot}88\times10^{-6}$	$6{\cdot}97\times10^{-2}$
3	$9{\cdot}07\times10^{-6}$	$4{\cdot}19\times10^{-7}$	$1{\cdot}15\times10^{-2}$
6	$4{\cdot}92\times10^{-6}$		$5{\cdot}26\times10^{-4}$
10	$3{\cdot}58\times10^{-6}$		$1{\cdot}48\times10^{-5}$
14	$3{\cdot}38\times10^{-6}$		$4{\cdot}60\times10^{-7}$
17	$9{\cdot}73\times10^{-7}$		

* Computing system solution by Gauss-Seidel method and Gauss elimination scheme took 0·792 and 2·457 s CPU time, respectively

(and, therefore, matrix entries in the same row) associated with the same distance R. We can write then

$$\sum_{j=1}^{n} |\mathrm{R}_{ij}| \leqslant \delta_i \sum_{k=1}^{m} \frac{1}{\mathrm{I}_{ik}^2}$$

where $m \leqslant n$, I_{ik} is an integer which is closest to the corresponding group of R's and δ_i is a constant which takes into account geometrical characteristics of the problem, boundary elements and repetition of distances prescribed to the corresponding integer I_{ik}.

Afterwards, we can obtain the following upper estimate:

$$\sum_{k=1}^{m} \frac{1}{\mathrm{I}_{ik}^2} \leqslant \sum_{I=1}^{\infty} \frac{1}{I^2} = \frac{\pi^2}{6}$$

Therefore,

$$\frac{\|\mathbf{q} - \bar{\mathbf{q}}\|}{\|\bar{\mathbf{q}}\|} \leqslant \|\mathbf{A}^{-1}\| \max_i(\delta_i) \frac{\pi^2}{6}$$

The upper part of Table III contains accuracy of the system solved keeping x per cent of matrix entries and number of iterations using CGS Method. In the numerical example mentioned at the beginning of this section, even if we keep 2 per cent of the total amount of matrix entries, we have got a difference between accurate ($x = 100$ per cent) and approximate solutions less then 3 per cent. The lower part of Table III contains circumferential stresses σ_θ at different cylinder sections. Values σ_θ {100 per cent} describe the case when all matrix entries are taken into consideration. Comparing the errors between solutions of the equations (upper part of Table III) and errors of stress σ_θ calculations, we can see that the order of these errors is approximately the same. As we use only small amount of matrix entries during iterative process, the smaller number of computational steps has to be done and, therefore, we may talk about a very cheap iterative solution which is proposed herein keeping reasonable accuracy of the results.

Table III. Accuracy of calculations with x per cent non-zero matrix coefficients

	$x = 100\%$	$x = 47\%$	$x = 27\%$	$x = 10\%$	$x = 2\%$
Accuracy $\delta\{x\%\} = \dfrac{\|\mathbf{b} - \mathbf{Aq}\|}{\|\mathbf{b}\|}$	$4{\cdot}19 \times 10^{-7}$	$1{\cdot}66 \times 10^{-5}$	$2{\cdot}27 \times 10^{-5}$	$1{\cdot}21 \times 10^{-4}$	$2{\cdot}23 \times 10^{-2}$
Number of iterations	3	2	2	1	1
Section number	$\sigma_\theta\{100\%\}$	Accuracy $\Delta\{x\%\} = \lvert\sigma_\theta\{100\%\} - \sigma_\theta\{x\%\}/\sigma_\theta\{100\%\}\rvert$			
		$\Delta\{47\%\}$	$\Delta\{27\%\}$	$\Delta\{10\%\}$	$\Delta\{2\%\}$
1	0·50	$9{\cdot}17 \times 10^{-6}$	$3{\cdot}06 \times 10^{-5}$	$3{\cdot}76 \times 10^{-5}$	$2{\cdot}23 \times 10^{-2}$
2	1.50	5.09×10^{-6}	1.92×10^{-5}	$1{\cdot}96 \times 10^{-5}$	$2{\cdot}23 \times 10^{-2}$
3	2·50	$5{\cdot}82 \times 10^{-6}$	$1{\cdot}99 \times 10^{-5}$	$1{\cdot}92 \times 10^{-5}$	$2{\cdot}23 \times 10^{-2}$
4	3·50	$4{\cdot}57 \times 10^{-6}$	$1{\cdot}87 \times 10^{-5}$	$1{\cdot}61 \times 10^{-5}$	$2{\cdot}23 \times 10^{-2}$
5	4·50	$1{\cdot}80 \times 10^{-6}$	$7{\cdot}31 \times 10^{-6}$	$6{\cdot}47 \times 10^{-6}$	$2{\cdot}23 \times 10^{-2}$

The type of the matrices allows us to conclude that for these and similar problems, it is possible to form sparse or even banded matrices instead of fully populated ones. Of course, in real problems, the band will be much wider than that presented in the numerical example. But the technique which employs the idea of forming a sparse matrix seems to be a way to model geometrically complicated problems in Mining and Civil Engineering with small memory and time requirements. Along with the above engineering problems, visible extensions can be made to model explicitly big amount of fractures and microcracks in mechanical structures. This motivates further investigation on a priori estimates of small matrix entries which can be neglected aimed to savings in computations.

ROCK SAMPLE

In this section, we consider a problem with more complicated geometry and boundary conditions. This research is aimed to model stresses which result in fracture propagation in a cubic rock sample (Figure 7(a)) in the course of laboratory experiments.[6] Each side of the cube has length of 20 cm. The sample is made of granite with nearly isotropic elastic properties (Young's modulus equals $E = 50$ GPA, Poisson's ratio equals $\nu = 0{\cdot}23$). The abscissa is perpendicular to the surface $AA'B'B$. The ordinate is perpendicular to the surface $BB'C'C$. A borehole is drilled along the axis Oz through the centre of the sample (Figure 7(b)). The radius r of the borehole is equal to $r = 0{\cdot}5$ cm. Two packers are used to create a chamber in the borehole[6] (Figures 7(c) and (d)).

During the laboratory experiments, the sample is first loaded by the normal external pressure through its surfaces $AA'B'B$, $BB'C'C$, $CC'D'D$, and $DD'A'A$. We call these sides as the external surface. Afterwards, water is pumped up to the chamber and the rock sample is loaded by additional internal pressure $-P_{\text{int}} = 22$ MPa (Figure 7(c)). Such a loading results in fracture that cuts the sample. If external pressure is small or equal to zero, the fracture propagates along the borehole. However, in the experiments with external pressure that is equal to $-P_{\text{ext}} = 8$ MPa, the fracture propagates perpendicular to the borehole axis.

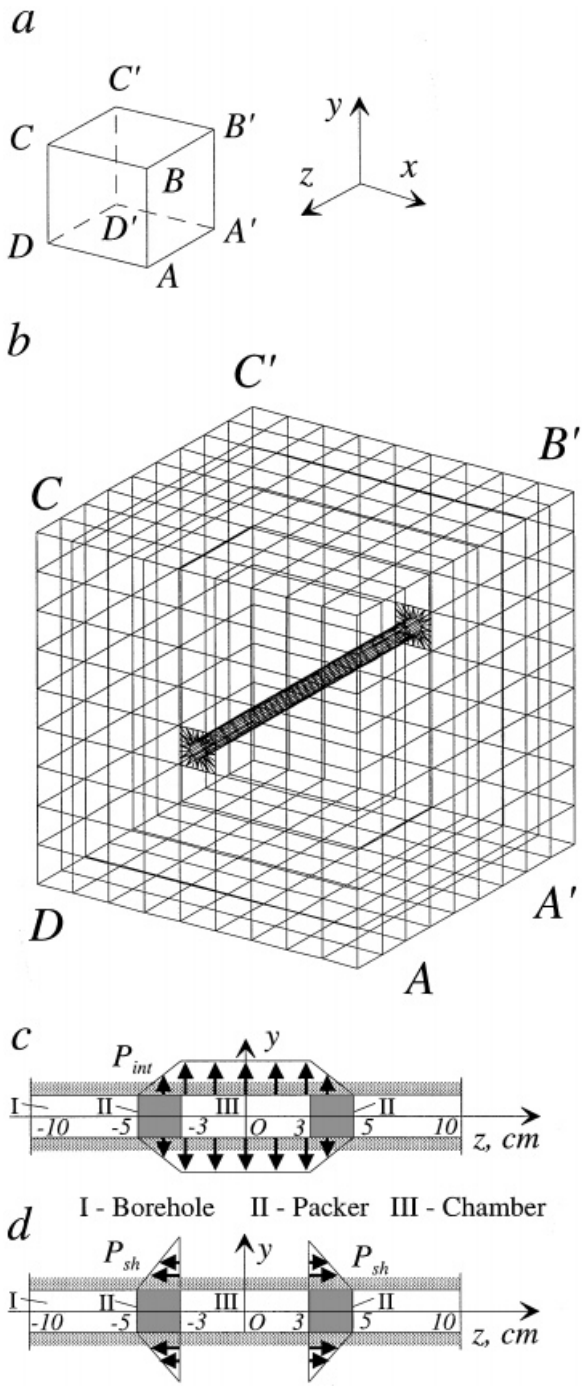

Figure 7. Rock sample and co-ordinate system (a), the mesh for the sample with the borehole (b), and boundary conditions on the borehole surface: normal P_{int} (c) and shear P_{sh} (d) loads, respectively

Table IV. Residuals at different stages of iterative solutions of 1300 linear simultaneous equations

Iteration number	Stress boundary conditions			Mixed boundary conditions		
	GSM	CGS	GMRES	GSM	CGS	GMRES
1	1·437	0·127	0·253	5·255	21·683	0·845
2	0·844	$7{\cdot}20\times10^{-2}$	0·123	6·841	1·008	0·305
3	0·364	$5{\cdot}73\times10^{-3}$	$2{\cdot}31\times10^{-2}$	4·134	0·196	0·151
4	0·120	$2{\cdot}74\times10^{-3}$	$9{\cdot}23\times10^{-3}$	1·878	$5{\cdot}33\times10^{-2}$	$7{\cdot}83\times10^{-2}$
6	$1{\cdot}20\times10^{-2}$	$2{\cdot}02\times10^{-4}$	$9{\cdot}16\times10^{-4}$	1·826	74·491	$1{\cdot}72\times10^{-2}$
8	$3{\cdot}62\times10^{-3}$	$9{\cdot}68\times10^{-7}$	$1{\cdot}13\times10^{-4}$	1·461	204·112	$6{\cdot}47\times10^{-3}$
13	$1{\cdot}79\times10^{-3}$		$8{\cdot}77\times10^{-7}$	0·855	1·163	$4{\cdot}59\times10^{-4}$
18	$1{\cdot}01\times10^{-3}$			0·496	$8{\cdot}91\times10^{-3}$	$1{\cdot}63\times10^{-5}$
22	$6{\cdot}44\times10^{-4}$			0·323	$6{\cdot}08\times10^{-8}$	$5{\cdot}71\times10^{-7}$
45	$5{\cdot}30\times10^{-5}$			$2{\cdot}76\times10^{-2}$		
102				$5{\cdot}30\times10^{-5}$		

We study influence of boundary conditions on the external surface on the stress field at the central area of the sample and analyse the following two cases:

1. SSS case. Stress boundary conditions on the external surface of the sample. Normal constant load $-P_{\text{ext}} = 8$ MPa and zero shear loads.
2. SDD case. Mixed boundary conditions on the external surface. Zero displacements on surfaces $AA'B'B$ and $DD'A'A$. Normal constant load $-P_{\text{ext}} = 8$ MPa and zero tangential displacements on surfaces $BB'C'C$ and $CC'D'D$.

Maximum value of internal pressure is equal to $-P_{\text{int}} = 22$ MPa, the influence of each packer is modelled by applying linear normal (Figure 7(c)) and linear shear ($P_{\text{sh}} = 0{\cdot}25P_{\text{int}}$, Figure 7(d)) loads along the axis Oz on the part of the borehole surface which contacted with the packers.[6] The sample surface was approximated by 1300 constant boundary elements (Figure 7(b)) that results in 3900 simultaneous linear equations. Table IV contains residuals at different stages of iterative solutions by Gauss–Seidel method (GSM), CGS, and GMRES methods for both SSS and SDD cases. We can observe that GSM has the lowest rate of convergence amongst of the methods used. CGS and GMRES methods demonstrate approximately equal convergence rate. However, GMRS method provides continuous decreasing of residuals while CGS method converges with rather big jumps in SDD case. We can also observe a natural fact that convergence in SSS case is faster than in SDD case. This is because all kernels decrease as $O(R^{-2})$ in SSS case and the most part of kernel functions in SDD case decrease as $O(R^{-1})$.

Table V contains accuracy of the system solved keeping x per cent if matrix entries and number of iterations using CGS Method. In the numerical example, if we keep 21 per cent of the total amount of matrix entries, we have got a difference between accurate ($x = 100$ per cent) and approximate solutions less then 3 per cent.

Stresses are calculated in the central area of the sample. In SSS case, the results of the computations are close to those received from the analytical solution of the plane strain problem, but with one exception. In the framework of the plane strain problem, $\sigma_z = \nu(\sigma_x + \sigma_y) = 3{\cdot}7$ MPa and according to this work we have $\sigma_z = 0{\cdot}5$ MPa. Maximum tensile stress on the borehole surface equals $\sigma_\theta = 5{\cdot}9$ MPa. In SDD case, we have got $12{\cdot}8\text{ MPa} < \sigma_\theta < 14{\cdot}7$ MPa and $-0{\cdot}2\text{ MPa} < \sigma_z < 0{\cdot}2$ MPa, respectively. According to this stress distribution, we may expect

Table V. Accuracy of calculations with x per cent non-zero matrix coefficients. Stress boundary conditions

	$x = 100\%$	$x = 47\%$	$x = 21\%$	$x = 1{\cdot}3\%$
Accuracy $\delta\{x\%\} = \dfrac{\|\mathbf{b} - \mathbf{Aq}\|}{\|\mathbf{b}\|}$	$9{\cdot}68 \times 10^{-7}$	$2{\cdot}37 \times 10^{-3}$	$2{\cdot}84 \times 10^{-2}$	0·369
Number of iterations	8	8	9	10

crack propagation along the borehole axis. However, in the experiments, it grows perpendicular to the borehole. In the authors' opinion, we will be able to explain the experimental data if we take into consideration existing microcracks and analyse stress intensity factors near to their edges. This analysis is planned to accomplish in the course of further research.[28,29]

CONCLUSIONS

Several approaches have been used to enhance the performance of the Indirect Boundary Element Method. One of them deals with application of efficient equation solvers. It was shown that Krylov-type methods like CGS and GMRES with simple Jacobi preconditioning appear to be efficient and robust. In addition, adaptive integration on the boundary elements, together with diagonal dominance of equations made it possible to accelerate convergence of the iterative procedure. Some of the problems discussed allowed a substantial reduction of matrix entries that led to a very cheap iterative solution keeping reasonable accuracy of the results. This motivates further investigation on a priori estimates of small matrix entries which can be neglected aimed to savings of the computer memory requirements.

ACKNOWLEDGEMENT

The work of M. A. Kayupov and V. E. Bulgakov has been sponsored by the Alexander von Humboldt Foundation (Germany). This support is gratefully acknowledged.

REFERENCES

1. S. M. Aitaliev, N. V. Banichuk and M. A. Kayupov, *Optimal Design of Extended Underground Structures*, Nauka, Alma-Ata, 1986 (in Russian).
2. S. L. Crouch and A. M. Starfield, *Boundary Element Methods in Solid Mechanics*, George Allen & Unwin, London, 1983.
3. Z. S. Erzhanov, Y. A. Veksler, N. A. Zhdankin and S. V. Kolokolov, *Mechanism of Dynamic Phenomena in Working Faces*, Nauka, Alma-Ata, 1984 (in Russian).
4. G. Hocking, 'Three-dimensional elastic stress distribution around the flat end of cylindrical cavity', *Int. J. Rock Mech. Mining Sci. & Geomech. Abstr.*, **13,** 331–337 (1976).
5. M. A. Kayupov, S. Sakurai and S. Akutagawa, 'BEM based calculating schemes for tunnels', in *Proc. 8th Int. Congress on Rock Mechanics*, Vol. 2, Tokyo, Japan, 1995, Balkema, Rotterdam, 1995, pp. 601–605.
6. M. A. Kayupov, G. Kuhn, T. Yamaguchi and M. Kuriyagawa, 'A coupled BE-DD method to model fracture propagation in rock samples and, *Proc. SARES 97: 1st Southern African Rock Engineering Symp.*, Johannesburg, South Africa, 1997, pp. 164–177.

7. K. Kuriyama and Y. Mizuta, 'Three-dimensional elastic analysis by the displacement discontinuity method with boundary division into triangular leaf elements', *Int. J. Rock Mech. Mining Sci. & Geomech. Abstr.*, **30** (2)**,** 111–123 (1993).
8. K. Kuriyama, Y. Mizuta, H. Mozumi and T. Watanabe, 'Three-dimensional elastic analysis by the Boundary Element Method with analytical integrations over triangular leaf elements', *Int. J. Rock Mech. Mining Sci. & Geomech. Abstr.*, **32** (1)**,** 77–83 (1995).
9. A. I. Lur'e, *Three-dimensional Problems of the Theory of Elasticity*, Interscience Publishers, Netherlands, 1964.
10. Y. Saad and M. H. Schultz, 'GMRES: A generalized minimal residual algorithm for solving nonsymmeytric linear systems', *SIAM J. Scient. Statist. Comput.*, **7,** 856–869 (1986).
11. P. Sonneveld, 'CGS, a fast Lanczos-type solver for nonsymmetric linear systems', *SIAM J. Sci. Stat. Comput.*, **10,** 36–52 (1989).
12. H. A. Van der Vorst, 'BiCGSTAB: a fast and smoothly converging variant of Bi-CG for the solution of nonsymmetric linear systems', *SIAM J. Scient. Statist. Comput.*, **13,** 631–644 (1992).
13. L. P. S. Barra, A. L. G. A. Coutinho, W. J. Mansur and J. C. F. Telles, 'Iterative solution of BEM equations by GMRES algorithm', *Comput. Struct.*, **44,** 1249–1253 (1992).
14. W. J. Mansur, F. C. Araujo and J. E. B. Malaghini, 'Solution of BEM systems of equations via iterative techniques', *Int. J. Numer. Meth. Engng.*, **33,** 1823–1844 (1992).
15. K. Guru Prasad, J. H. Kane, D. E. Keyes and C. Balakrishna, 'Preconditioned Krylov solvers for BEA', *Int. J. Numer. Meth. Engng.*, **37,** 1651–1672 (1994).
16. M. Hribersek and L. Skerget, 'Iterative methods in solving Navier–Stokes equations by the boundary element method', *Int. J. Numer. Meth. Engng.*, **39,** 115–139 (1996).
17. V. E. Bulgakov, M. Merkel, R. A. Bialecki and G. Kuhn, 'On the iterative solution of the large-scale BEM industrial problems', submitted.
18. P. Sonneveld, P. Wesseling and P. M. de Zeeuw, 'Multigrid and conjugate gradient methods as convergence acceleration techniques', in D. J. Paddon and H. Holstein (eds.), *Multigrid Methods for Integral and Differential Equations*, Clarendon Press, Oxford, 1985, pp. 117–167.
19. V. E. Bulgakov, B. Sarler and G. Kuhn, 'Iterative solution of systems of equations in dual reciprocity boundary element method for diffusion equation', *Int. J. Numer. Meth. Engng.*, submitted.
20. A. Y. Alexandrov, 'Solution of main three-dimensional problems of the elasticity theory by numerical implementation of the integral equations method' *Reports of the Academy of Sciences of the USSR*, Vol. 208, 1973, pp. 291–294 (in Russian).
21. Y. V. Veryuzhskii, *Use of the Potential Method to Solve Problems of Theory of Elasticity* (in Russian), Kiev Institute for Civil Engineering, KISI, Kiev, 1975.
22. P. Partheymüller, R. A. Bialeki and G. Kuhn, 'Self-adapting algorithm for evaluation of weakly singular integrals arising in the boundary element method', *Engng. Anal. Boundary Elements*, **14,** 285–292 (1994).
23. T. Wiles, *MAP3D^{PV} User Manual*, Mine Modelling Limited, Copper Cliff, 1992.
24. N. I. Antonov and B. M. Zinov'ev, 'Exact and confidant solutions for the problem of distributed loads in an elastic medium and plane', in *Solid Mechanics and Transport Constructions Design*, NIIJT, Novosibirsk, 1978, pp. 68–79 (in Russian).
25. B. W. Char *et al.*, *MAPLE 5, Library Reference Manual*, Springer, Berlin, 1991.
26. V. E. Bulgakov, 'On the two-grid approximate approach for constructing sparse boundary systems in substructuring', *Comput. Struct.*, **49,** 3, 391–398 (1993).
27. V. E. Bulgakov, R. A. Bialecki and G. Kuhn, 'Coarse division transform based preconditioner for boundary element problems', *Int. J. Num. Meth. Engng.*, **38,** 2115–2129 (1995).
28. M. A. Kayupov, P. Partheymüller, G. Kuhn, T. Yamaguchi and M. Kuriyagawa, 'Numerical modelling of 3-D cracks created during laboratory experiments on hydrofracturing', to be submitted.
29. M. A. Kayupov, P. Partheymüller, G. Kuhn, T. Yamaguchi and M. Kuriyagawa, 'Hydraulic pressure induced crack orientations in strained rock samples', *NARMS '98 – the 3rd North American Rock Mechanics Symp.*, Cancun, Mexico, 1998, to be presented.

